The Astrophysics of Planetary Systems: Formation, Structure, and Dynamical Evolution
Proceedings IAU Symposium No. 276, 2010
A. Sozzetti, M. G. Lattanzi & A. P. Boss, eds.

doi:10.1017/S1743921311019995

High-resolution simulations of planetesimal formation in turbulent protoplanetary discs

Anders Johansen[1], Hubert Klahr[2] and Thomas Henning[2]

[1]Lund Observatory, Lund University
Box 43, 221 00 Lund, Sweden
email: anders@astro.lu.se

[2]Max-Planck-Institut für Astronomie
Königstuhl 17, 69117 Heidelberg, Germany

Abstract. We present high resolution computer simulations of dust dynamics and planetesimal formation in turbulence triggered by the magnetorotational instability. Particles representing approximately meter-sized boulders clump in large scale overpressure regions in the simulation box. These overdensities readily contract due to the combined gravity of the particles to form gravitationally bound clusters with masses ranging from a few to several ten times the mass of the dwarf planet Ceres. Gravitationally bound clumps are observed to collide and merge at both moderate and high resolution. The collisional products form the top end of a distribution of planetesimal masses ranging from less than one Ceres mass to 35 Ceres masses. It remains uncertain whether collisions are driven by dynamical friction or underresolution of clumps.

Keywords. accretion, accretion disks, MHD, turbulence, planetary systems: formation, planetary systems: protoplanetary disks

1. Introduction

The formation of km-scale planetesimals from dust particles involves a complex interplay of physical processes, including most importantly collisional sticking (Weidenschilling 1997; Dullemond & Dominik 2005), the self-gravity of the sedimentary particle mid-plane layer (Safronov 1969; Goldreich & Ward 1973; Sekiya 1998; Youdin & Shu 2002; Johansen *et al.* 2007), and the motion and structure of the turbulent protoplanetary disc gas (Weidenschilling & Cuzzi 1993; Johansen *et al.* 2006; Cuzzi *et al.* 2008).

In the initial growth stages micrometer-sized silicate monomers readily stick to form larger dust aggregates (Blum & Wurm 2008). Further growth towards macroscopic sizes is hampered by collisional fragmentation and bouncing (Zsom *et al.* 2010), limiting the maximum particle size to a few cms or less. High speed collisions between a small impactor and a large target constitutes a path to net growth (Wurm *et al.* 2005), but the separation of small particles from large particles by turbulent diffusion limits the resulting growth rate (Johansen *et al.* 2008). Material properties are also important. Wada *et al.* (2009) demonstrated efficient sticking between ice aggregates consisting of 0.1 μm monomers at speeds up to 50 m/s.

Turbulence can play a positive role for growth by concentrating mm-sized particles on small scales (Cuzzi *et al.* 2008), near the dissipative scale of the turbulence, and m-sized particles on large scales in long-lived geostrophic pressure bumps surrounded by axisymmetric zonal flows (Johansen *et al.* 2009a). In the model presented in Johansen *et al.* (2007) approximately meter-sized particles settle to form a thin mid-plane layer in balance between sedimentation and turbulent stirring. Particles then concentrate in nearly axisymmetric gas high pressure regions, reaching local column densities up to ten

times the average. The gravitational attraction between the particles in these overdense regions is high enough to initiate first a slow radial contraction, and as the local mass density becomes comparable to the Roche density, a full non-axisymmetric collapse to form gravitationally bound clumps with masses comparable to the dwarf planet Ceres.

Some of the open questions related to this gravoturbulent picture of planetesimal formation is to what degree the planetesimal size spectrum is numerically converged and the possible role of collisions and coagulation during the clumping and the gravitational collapse. Following a burst of planetesimal formation, the initial mass function can evolve rapidly by planetesimal mergers and accretion of unbound particles. Exploring the role of such physical effects requires both increased spatial resolution and increased simulation time.

In this paper we present high resolution and long time integration simulations of planetesimal formation in turbulence caused by the magnetorotational instability (MRI). We present the first evidence for collisions between newly formed planetesimals, observed at both moderate and high resolution, and indications that the initial mass function of planetesimals involve masses ranging from a few to several ten Ceres masses.

2. Simulation set up

We perform simulations solving the standard shearing box MHD/drag force/self-gravity equations for gas defined on a fixed grid and solid particles evolved as numerical superparticles. We use the Pencil Code, a sixth order spatial and third order temporal symmetric finite difference code†. The shearing box coordinate frame rotates at the Keplerian frequency Ω at an arbitrary distance r_0 from the central star. The axes are oriented such the x points radially away from the central gravity source, y points along the Keplerian flow, while z points vertically out of the plane.

Particle collisions become important inside dense particle clumps. In Johansen *et al.* (2007) the effect of particle collisions was included in a rather crude way by reducing the relative rms speed of particles inside a grid cell on the collisional time-scale, to mimic collisional cooling. Recently Rein *et al.* (2010) found that the inclusion of particle collisions changes the structure of small scale self-gravitating clumps that condense out of a turbulent flow.

Lithwick & Chiang (2007) presented a Monte Carlo method for superparticle collisions whereby the correct collision frequency can be obtained by letting nearby superparticle pairs collide on the average once per collisional time-scale. We have implemented this method in the Pencil Code and will present the algorithm and numerical tests in a paper in preparation (Johansen, Youdin, & Lithwick, in preparation). We let a particle interact with all other particles in the same grid cell. The collision time-scale $\tau_{\rm coll}$ between all particle pairs is calculated, and for each possible collision a random number P is chosen. If P is smaller than $\delta t/\tau_{\rm coll}$, where δt is the time-step set by the magnetohydrodynamics, then the two particles collide. The collision outcome is determined as if the two superparticles were actual particles with radii large enough to touch each other. By solving for momentum conservation and energy conservation, with the possibility for inelastic collisions to dissipate kinetic energy to heat and deformation, the two colliding particles acquire their new velocity vectors instantaneously.

All simulations include collisions with a coefficient of restitution of $\epsilon = 0.3$, meaning that each collision leads to the dissipation of approximately 90% of the relative kinetic energy to deformation and heating of the colliding boulders.

† See `http://code.google.com/p/pencil-code/`.

https://doi.org/10.1017/S1743921311019995 Published online by Cambridge University Press

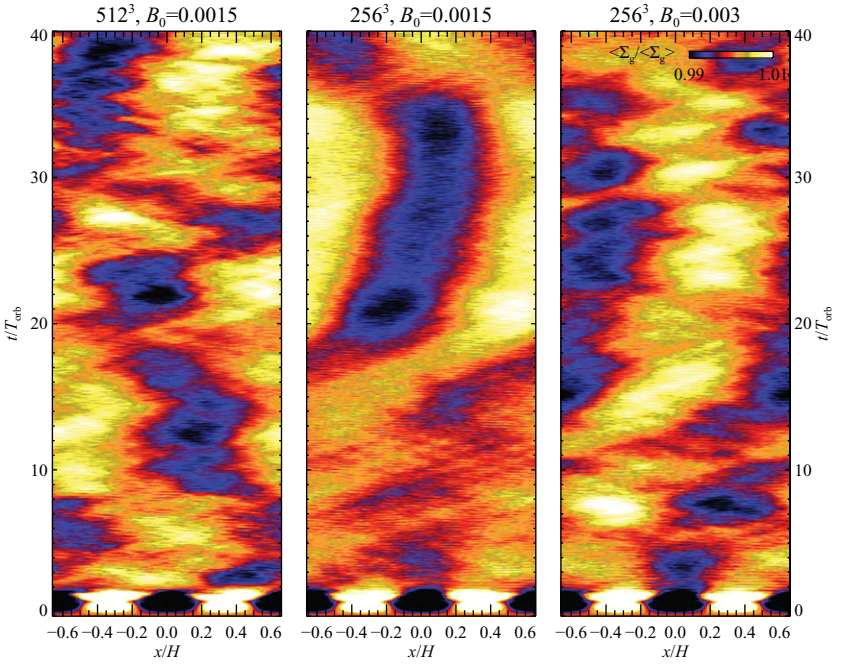

Figure 1. The gas column density averaged over the azimuthal direction, as a function of radial coordinate x and time t in orbits. Large scale pressure bumps appear with approximately 1% amplitude at both 256^3 and 512^3 resolution.

3. Results

An important feature of magnetorotational turbulence is the emergence of large scale slowly overturning pressure bumps (Fromang & Nelson 2005; Johansen *et al.* 2006). Large particles – pebbles, rocks, and boulders – are attracted to the center of pressure bumps, because of the drag force associated with the sub-Keplerian/super-Keplerian zonal flow envelope. In presence of a mean radial pressure gradient the trapping zone is slightly downstream of the pressure bump, where there is a local maximum in the combined pressure.

An efficient way to detect pressure bumps is to average the gas density field over the azimuthal and vertical directions. In Figure 1 we show the gas column density in the 256^3 and 512^3 simulations averaged over the y-direction, as a function of time. Large scale pressure bumps are clearly visible, with spatial correlation times of approximately 10-20 orbits. The pressure bump amplitude is around 1%, independent of both resolution and strength of the external field.

We release the particles at a time when the turbulence has saturated, but choose a time when there is no significant large scale pressure bump present. Thus we choose $t = 20T_{\rm orb}$ for the 256^3 simulation and $t = 32T_{\rm orb}$ for the 512^3 simulation (see Figure 1).

The particles immediately fall towards the mid-plane of the disc, before finding a balance between sedimentation and turbulent stirring. Figure 2 shows how the presence of gas pressure bumps has a dramatic influence on particle dynamics. The particles display column density concentrations of up to 4 times the average density just downstream of the pressure bumps. At this point the gas moves close to Keplerian, because the pressure gradient of the bump balances the radial pressure gradient there. The column density concentration is relatively independent of the resolution, as expected since the pressure bump amplitude is almost the same.

https://doi.org/10.1017/S1743921311019995 Published online by Cambridge University Press

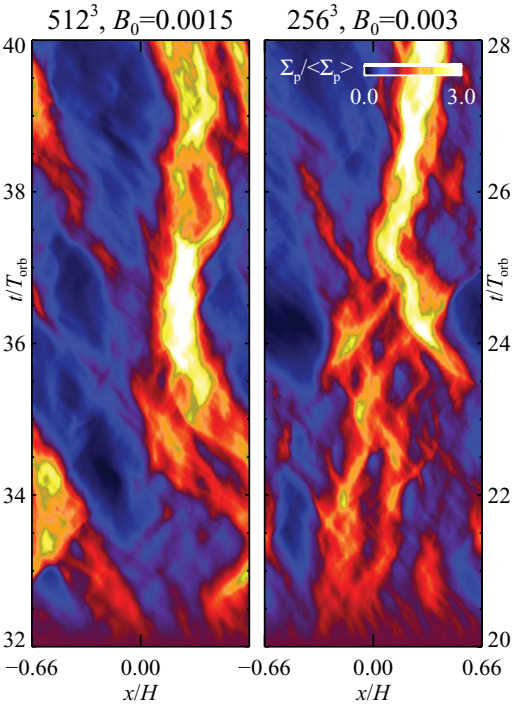

Figure 2. The particle column density averaged over the azimuthal direction, as a function of radial coordinate x and time t in orbits. The starting time was chosen to be slightly prior to the emergence of a pressure bump. The particles concentrate slightly downstream of the gas pressure bump, with a maximum column density between three and four times the mean particle column density.

A simulation including the self-gravity of the particles is presented in Figure 3. The Hill sphere of each bound clump is indicated in Figure 3, together with the mass of particles encompassed inside the Hill radius (in units of the mass of the dwarf planet Ceres)

4. Conclusions

At both moderate and high resolution we observe the close approach and merging of gravitationally bound clumps. Some concerns remain about whether these collisions are real, since our particle-mesh self-gravity algorithm prevents bound clumps from being smaller than a grid cell. Thus the collisional cross section is artifically large. Two observations nevertheless indicate that the collisions may be real: we observe planetesimal mergers at both moderate and high resolution and we see that the environment in which planetesimals merge is rich in unbound particles. Dynamical friction may thus play an important dissipative role in the dynamics and the merging (Goldreich *et al.* 2002).

The measured α-value of MRI turbulence at 512^3 is $\alpha \approx 0.003$. At a sound speed of $c_{\rm s} = 500$ m/s, the expected collision speed of marginally coupled m-sized boulders is $\sqrt{\alpha} c_{\rm s} \approx 25 - 30$ m/s. Johansen *et al.* (2007) showed that the actual collision speeds can be a factor of a few lower, because the particle layer damps MRI turbulence locally. In general boulders are expected to shatter when they collide at 10 m/s or higher (Benz 2000). Much larger km-sized bodies are equally prone to fragmentation as random gravitational torques exerted by the turbulent gas excite relative speeds higher than the gravitational escape speed (Ida *et al.* 2008; Leinhardt & Stewart 2009). A good environment for

https://doi.org/10.1017/S1743921311019995 Published online by Cambridge University Press

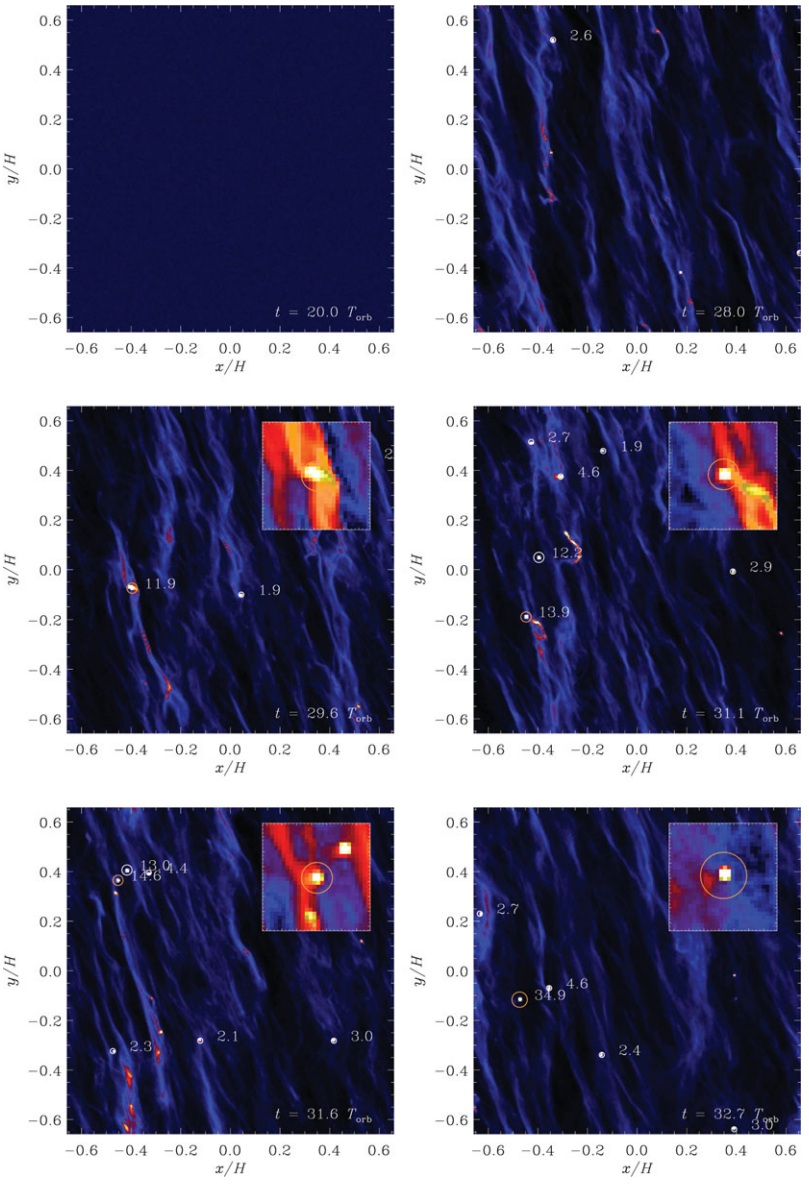

Figure 3. The particle column density as a function of time after self-gravity is turned on at $t = 20.0T_{\rm orb}$ for a simulation with 256^3 grid cells and 8×10^6 particles. The insert shows an enlargement of the region around the most massive bound clump. Each clump is labelled by its Hill mass in units of Ceres masses. The most massive clump at the end of the simulation contains a total particle mass of 34.9 Ceres masses, partially as the result of a collision between a 13.0 and a 14.6 Ceres mass planetesimal occuring at a time around $t = 31.6T_{\rm orb}$.

building planetesimals from boulders may require $\alpha < 0.001$. Johansen *et al.* (2009b) presented simulations with no MRI turbulence where turbulence and particle clumping is driven by the streaming instability (Youdin & Goodman 2005). They found typical collision speeds as low as a few meters per second.

A second reason to prefer weak turbulence is the amount of mass available in the disc. If we apply our results to $r = 5\,{\rm AU}$, then our dimensionless gravity parameter corresponds

https://doi.org/10.1017/S1743921311019995 Published online by Cambridge University Press

to a gas column density of $\Sigma_{\rm gas} \approx 1500\,{\rm g\,cm^{-2}}$, ten times higher than the Minimum Mass Solar Nebula (Hayashi 1981). Turbulence driven by streaming instability and Kelvin-Helmholtz instability can form planesimals for column densities comparable to the Minimum Mass Solar Nebula (Johansen *et al.* 2009b). Thus even moderate amounts of MRI turbulence seems to have an overall negative effect on the ability of the particle layer to undergo gravitational collapse and on the survival of boulders and planetesimals in face of shattering collisions.

5. Acknowledgements

This project was made possible through a computing grant for five rack months at the Jugene BlueGene/P supercomputer at Research Center Jülich. Each rack contains 4096 cores, giving a total computing grant of approximately 15 million core hours. We are grateful to Tristen Hayfield for discussions on particle load balancing.

References

Benz, W. 2000, *SSRv*, 92, 279
Blum, J. & Wurm, G. 2008, *ARA&A*, 46, 21
Cuzzi, J. N., Hogan, R. C., & Shariff, K., 2008, *ApJ*, 687, 1432
Dullemond, C. P. & Dominik, C. 2005, *A&A*, 434, 971
Fromang, S. & Nelson, R. P. 2005, *MNRAS*, 364, L81
Goldreich, P. & Ward, W. R. 1972, *ApJ*, 183, 1051
Goldreich, P., Lithwick, Y., & Sari, R. 2002, *Nature*, 420, 643
Hayashi, C. 1981, *Progress of Theoretical Physics Supplement*, 70, 35
Ida, S., Guillot, T., & Morbidelli, A. 2008, *ApJ*, 686, 1292
Johansen, A., Klahr, H., & Henning, Th. 2006, *ApJ*, 636, 1121
Johansen, A., Oishi, J. S., Low, M., Klahr, H., Henning, Th., & Youdin, A. 2007, *Nature*, 448, 1022
Johansen, A., Brauer, F., Dullemond, C., Klahr, H., & Henning, T. 2008, *A&A*, 486, 597
Johansen, A., Youdin, A., & Klahr, H. 2009a, *ApJ*, 697, 1269
Johansen, A., Youdin, A., & Mac Low, M.-M. 2009b, *ApJL*, 704, L75
Leinhardt, Z. M. & Stewart, S. T. 2009, *Icarus*, 199, 542
Lithwick, Y. & Chiang, E. 2007, *ApJ*, 656, 524
Rein, H., Lesur, G., & Leinhardt, Z. M. 2010, *A&A*, 511, A69
Safronov, V. S. 1969, *Evoliutsiia doplanetnogo oblaka* (English transl.: Evolution of the Protoplanetary Cloud and Formation of Earth and the Planets, NASA Tech. Transl. F-677, Jerusalem: Israel Sci. Transl. 1972)
Sekiya, M. 1998, *Icarus*, 133, 298
Youdin, A. N. & Shu, F. H. 2002, *ApJ*, 580, 494
Youdin, A. N. & Goodman, J. 2005, *ApJ*, 620, 459
Wada, K., Tanaka, H., Suyama, T., Kimura, H., & Yamamoto, T. 2009, *ApJ*, 702, 1490
Weidenschilling, S. J. & Cuzzi, J. N. 1993, in *Protostars and Planets III*, 1031
Weidenschilling, S. J. 1997, *Icarus*, 127, 290
Wurm, G., Paraskov, G., & Krauss, O. 2005, *Icarus*, 178, 253
Zsom, A., Ormel, C. W., Güttler, C., Blum, J., & Dullemond, C. P. 2010, *A&A*, 513, A57